High-Response Electromechanical Control Actuator

G. D. Goldshine and G. T. Lacy
General Dynamics Corporation
Pomona, California

Because the need for advanced missile system performance required increased propulsion space, the space available in the missile for the control section was decreased by two-thirds. At the same time, long-term storage without maintenance required an all-electric control system. Prime objectives were to achieve substantial weight, power, and cost reductions while attaining significant increase in control capability. The resulting design of a high-performance electromechanical actuator developed at the Pomona Division of General Dynamics is described. An analytical model for investigating the internal characteristics of the actuator is shown, and some significant performance features are discussed. Development flight testing of the system has been completed, and the actuator is being mass-produced in the STANDARD MISSILE and ARM programs.

I. Introduction

The increased performance requirements for tactical missile systems initiated the development of adaptive control techniques for achieving the control-system parameter requirements. Before these techniques could be applied, a bistable control actuator with performance characteristics exceeding those available from any previous actuator development was required. The present study developed such an electromechanical actuator.

II. System Constraints

There were three principal system constraints on the control actuator:

(1) The reduced space envelope.

(2) The reduction in weight.

(3) The control parameters.

A. Space Envelope

The basic necessity for increasing advanced missile system performance dictated the need for increased propulsion system performance. The propulsion increase was gained by the use of a longer rocket motor. Since the overall missile was not elongated, it became necessary to package the control section in a space envelope approximately two-thirds the length of previous section volumes. At the same time, from the standpoint of maintainability and producibility, it was necessary to provide a modular design that would be packaged by quadrant, so that four identical actuators were provided per missile. (The missile is controlled by four tail control surfaces, each driven by a separate actuator.)

B. Weight

Each actuator weighs approximately 12.8 lb; the entire control section weighs 68 lb, which represents about a

40% reduction in weight from the control section previously used in missile designs.

C. Control Parameters

The principal control parameters for the electromechanical actuator are given in Table 1.

Table 1. Control parameters

Parameter	Requirement
Transport delay time (from applied control signal to actuator reversal at full rate)	3 ±1 ms
No-load tail rate	200 ±50 deg/s
Tail drift rate (under no-load conditions in the bistable open-loop mode)	≤ 5 deg/s
Input power (nominal/ambient)	520 W
Load sensitivity (tail drift rate/in.-lb of applied external hinge moment)	0.05 deg/s/in.-lb
Operating life cycle (3 min *on*, 60 min *off*; 4 min for ARM)	1 h total on time

III. System Description

Each actuator, in combination with a bistable switching amplifier situated in the autopilot electronics, operates in a bistable mode such that the output is a maximum CW or CCW rate of change of tail incidence angle. The overall missile control system is adaptive by virtue of including the bistable switch/actuator combination in cascade with the missile dynamics in a closed loop, such that a limit cycle mode is sustained. Changes in gain in the forward path of the loop (i.e., aerodynamic parameter changes) will then be automatically compensated for by a resulting inverse change of nonlinear gain in the bistable switch/actuator combination. The limit cycle characteristics are fully determined only by including missile loop parameters together with the internal dynamics of the actuators themselves. (A full description of the adaptive loop is outside the scope of this paper.) The absence of the more conventional closed-loop position feedback directly around the actuator also introduces a need for special consideration of tail position drift errors due to internal unbalance within the actuators and external loading applied to the tails.

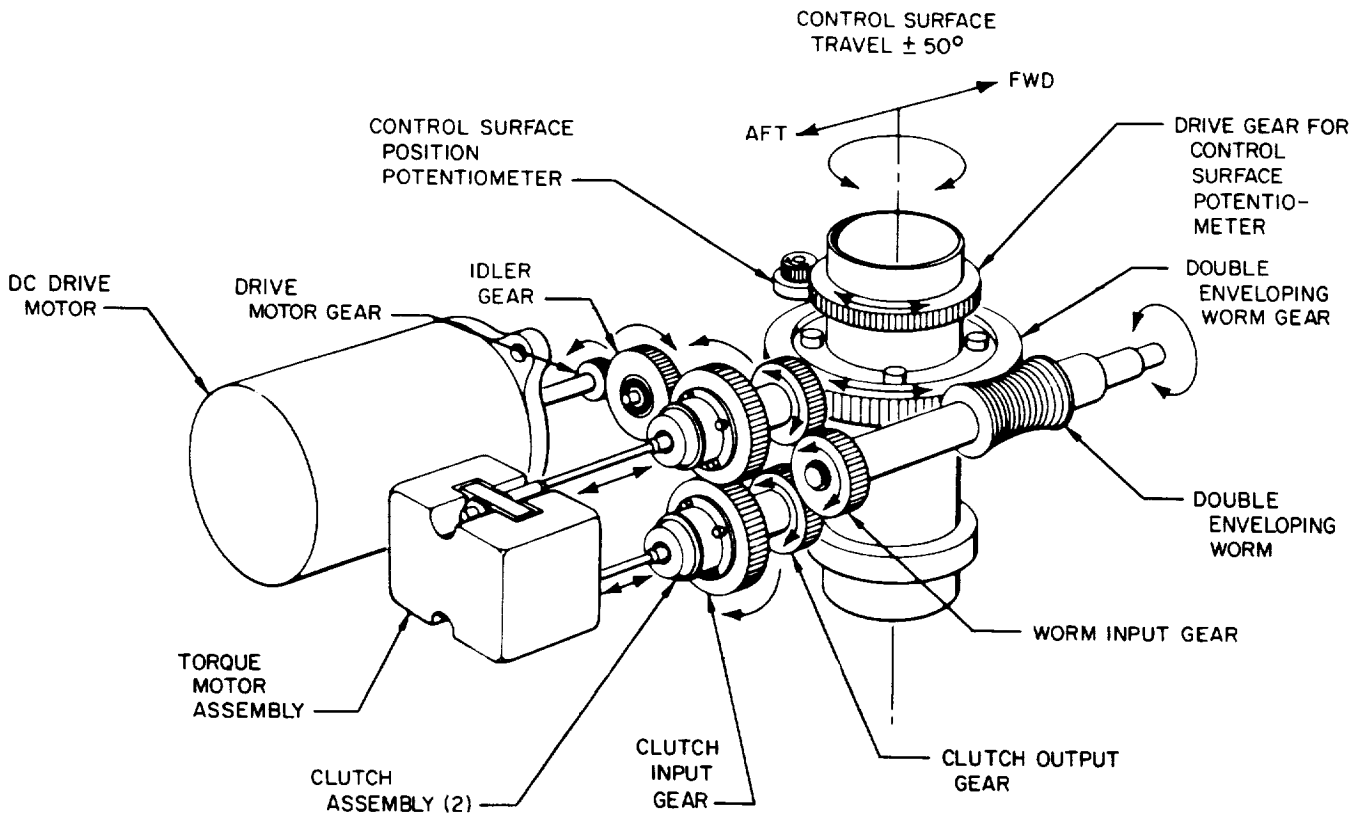

Fig. 1. Actuator mechanical schematic

The electromechanical actuator consists of the following parts: two contra-rotating capstan spring clutches with actuating cones, a torque motor, a unidirectional dc drive motor, a reduction gear train, a worm output drive, and a control surface position potentiometer (see Fig. 1).

Operation of the actuator is as follows: the contra-rotating clutch input gears that mount the capstan springs are driven at an essentially constant speed by the drive motor and reduction gear train. Both clutch output shafts are geared through a further spur gear stage to a single worm shaft. The actuator output shaft carries a sector gear in mesh with the worm and provides a direct mounting for the aerodynamic control surface. Engagement of either one of the clutches closes the drive path between the drive motor and the control surface (tail), thus imparting maximum velocity to the surface in a direction depending upon which clutch is engaged.

IV. Analytical Model

An analytical model of the system suitable for analog computer simulation was developed, as shown in Fig. 2.

A. Drive Motor

The torque developed as a function of applied voltage and rotational speed may be expressed approximately as

$$M_e = N_1 \frac{K_T}{R} (V_e - K_b N_1 \dot{\theta}_e)$$

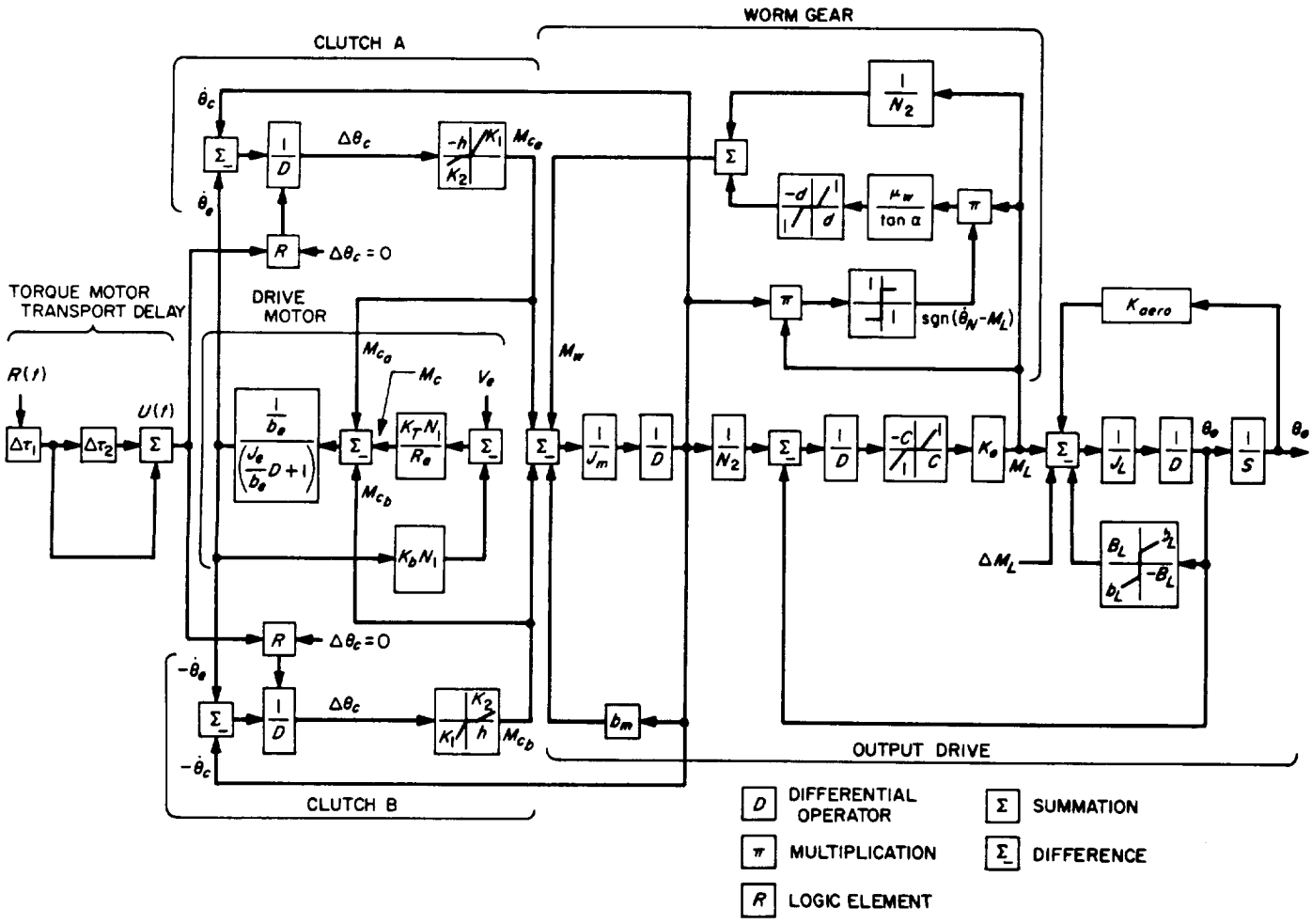

Fig. 2. Functional block diagram, electromechanical clutch actuator

Inertia and viscous friction of the unidirectional rotating parts are considered as lumped parameters J_e and b_e. Further neglecting compliance and backlash in this part of the drive, the velocity of the clutch input gears may be written

$$\dot{\theta}_e = \frac{\frac{1}{b_e}}{\left(\frac{J_e}{b_e} D + 1\right)} (M_e - M_c)$$

B. Clutch

Each clutch is represented in both the engaged and disengaged modes. In the disengaged mode, no contact is possible between spring and clutch output and, therefore, no torque is transmitted. In the engaged mode, the clutch cone is assumed to be fully depressed by the torque motor so as to accomplish complete coil windup, and maximum torque is transmitted in accordance with the clutch torsional stiffness K_1.

C. Torque Motor

The torque motor function is expressed as a pure transport delay time of $\Delta\tau_1$ and $\Delta\tau_2$ as follows:

$\Delta\tau_1$ = time from application of input voltage to first armature motion

$\Delta\tau_2$ = time to transfer the engagement mode from one clutch to the other

The output $U(t)$ is used on the control signal for the engagement/disengagement mode and is depicted as a square wave of dead time ($\Delta\tau_1$) and phase lag ($\Delta\tau_2$) with respect to a driver signal $R(T)$.

D. Worm Gear

The characteristic of coulomb friction at the worm mesh is depicted here. Since this is dependent on the magnitude of transmitted torque, it can be expressed as

$$M_w = \frac{M_L}{N_2}\left[1 - \frac{\mu_w}{\tan\alpha} \cdot \text{sgn}\,(\dot{\theta}_w \cdot M_L)\right]$$

where

sgn (M_L) = sgn (θ_w) when load torque is in the direction of rotation

sgn (M_w) = sgn (M_L) when the input torque is opposite to the load torque.

E. Output Drive

All of the reversing parts of the actuator are included here. Backlash and compliance are assumed across the worm mesh in combination with inertia and friction on each side of the mesh. Then the clutch output torque can be expressed as

$$M_c = (J_m D + b_m)\,\dot{\theta}_c + M_w$$

and torque developed at the worm mesh output can be depicted as

$$M_L = J_L D\dot{\theta}_o + b_L\dot{\theta} + B_L \text{ sgn } \dot{\theta}_o$$

Owing to drive backlash and compliance, the angular deflection between the actuator output shaft and worm output gear may be expressed as

$$\theta_o = \frac{1}{D}\left(\frac{\dot{\theta}_w}{N_2} - \dot{\theta}_o\right)$$

The torque transmitted across the drive may be written as

$$M_L = K_o\,(\Delta\theta_o - C), \qquad \Delta\theta_o > C$$

and

$$M_L = 0, \qquad \Delta\theta_o < C$$

One of the prime factors of the computer study has been to investigate the effect of various parameters on waveform and torque sensitivity. The internal dynamics of the actuator are severely affected by the friction in the various stages of the mechanism which, in turn, affect the distortion characteristic of the actuator output. A typical computer run is shown in Fig. 3. The dynamic overshoot characteristics of the clutch output velocity are illustrated. This occurs because of the release of strain energy during the engagement and the backing-off of the spring as the output velocity exceeds the input. Thus, the clutches transmit torque in very sharp impulses.

In general, the frictional characteristics of the output shaft bearings appear to have the greatest effect on the waveform characteristics of the actuator.

Typical computer results for actuator characteristics under hinge moment loading are shown in Fig. 4. The knee is a strong function of μ_w (worm mesh friction).

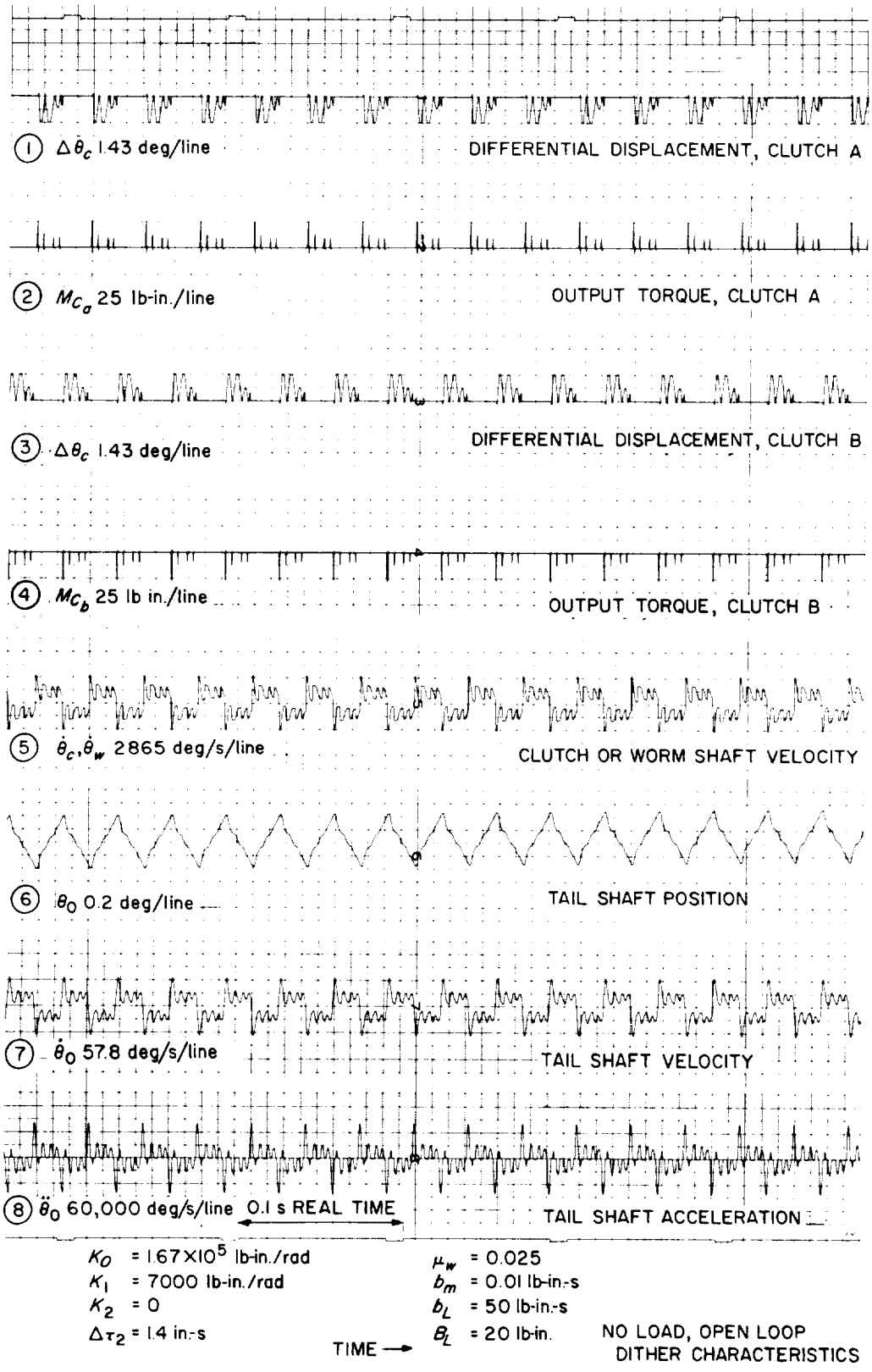

Fig. 3. Typical computer run, actuator output

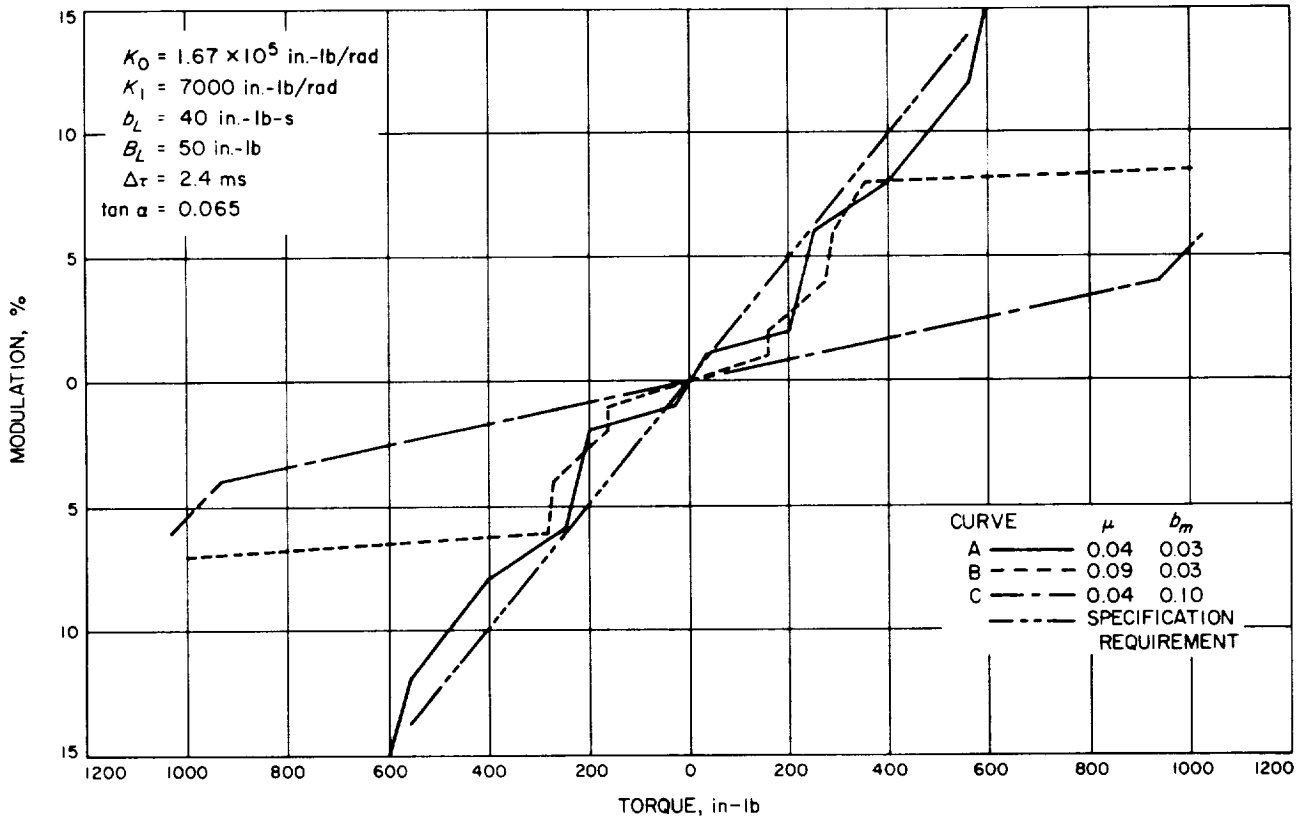

Fig. 4. Analytical hinge moment characteristic

V. Performance Characteristics

The basic characteristic parameters of the actuator fall in the category of waveform shape, power input and output, torque motor performance, transport delay time, drift, and torque sensitivity.

A typical performance trace of a developmental model under no-load operating conditions is shown in Fig. 5. Of prime interest here is the smooth trace and the operation of the actuator within the transport delay time, consistently and repeatably. The tail-rate performance is well within specification for all conditions.

The basic necessity for the hinge-moment sensitivity requirement is to control the drift of the actuator under hinge-moment loading effect. This requirement results from the method of utilizing the actuator in an effective open-loop operation as part of the adaptive control technique. The actuator's sensitivity to drift is accented by the differential number of clutch engagements in each half cycle. Under loading effects which either aid or oppose the actuator motion during the cycle, there is a resultant drift known as hinge-moment sensitivity.

The effect of actuator parameters on hinge-moment sensitivity is shown in Fig. 4, taken from the computer simulation. For case A where $\mu_{ic} < \tan \alpha$, a steep slope indicates a strong influence of external torque. Case B for $\mu_{ir} > \tan \alpha$ (i.e., irreversible worm condition) has the characteristic knee. Performance is improved for higher torques, indicated by the flatter slope beyond the knee. A reduction of μ_{ic} and an increase in viscous friction b_m at the worm shaft, in C, results in a flat slope throughout the design torque range. The increase in b_m is obtained by including a simple plate damper to the worm shaft. Typical actuator test data, with and without the dampers, are shown in Fig. 6. Computer data points also included in Fig. 6 show good correlation between the test data and theoretical results.

VI. Program Status

The present program has undergone flight testing of development prototype missiles. This is, in essence, a preproduction evaluation program leading to final production models.

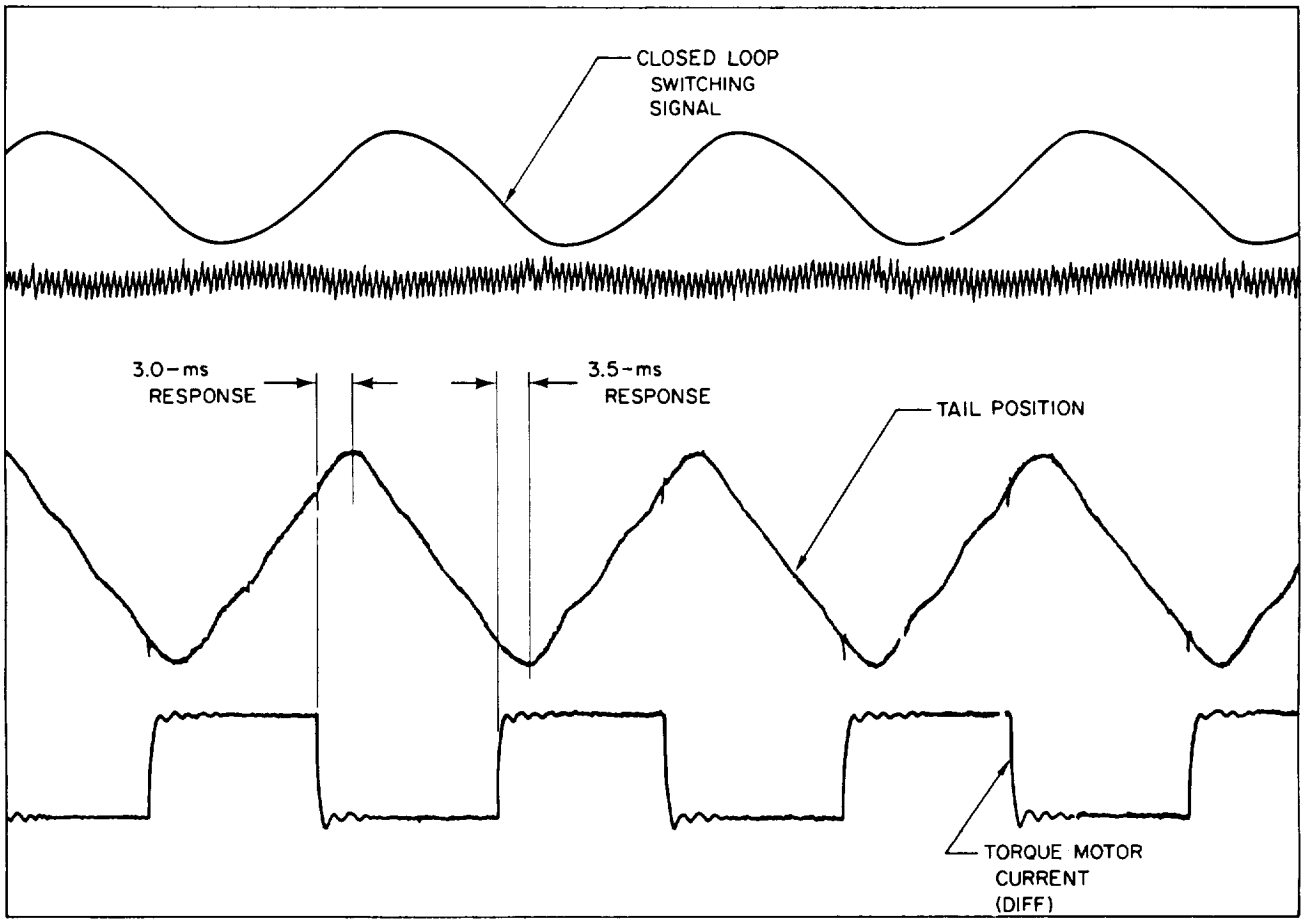

Fig. 5. Typical waveform diagram

The actuator is fully developed and qualified. It is in current production on the STANDARD ARM and STANDARD MISSILE programs. The number of production units manufactured is in excess of 700 devices.

Nomenclature

b_e	drive motor friction, viscous
b_L	output shaft friction, viscous
b_m	clutch + worm shaft friction, viscous
B_L	output shaft friction, coulomb
C	output drive backlash
d	displacement
D	differential operator
J_e	drive motor inertia
J_L	output shaft inertia
J_m	clutch + worm shaft inertia
K_o	output drive stiffness
$K_{1,2}$	clutch spring stiffness
K_{aero}	external load spring constant
K_b	drive motor back emf
K_T	drive motor torque sensitivity
M_c	clutch output torque
M_e	drive motor torque at the clutch
M_L	external load torque

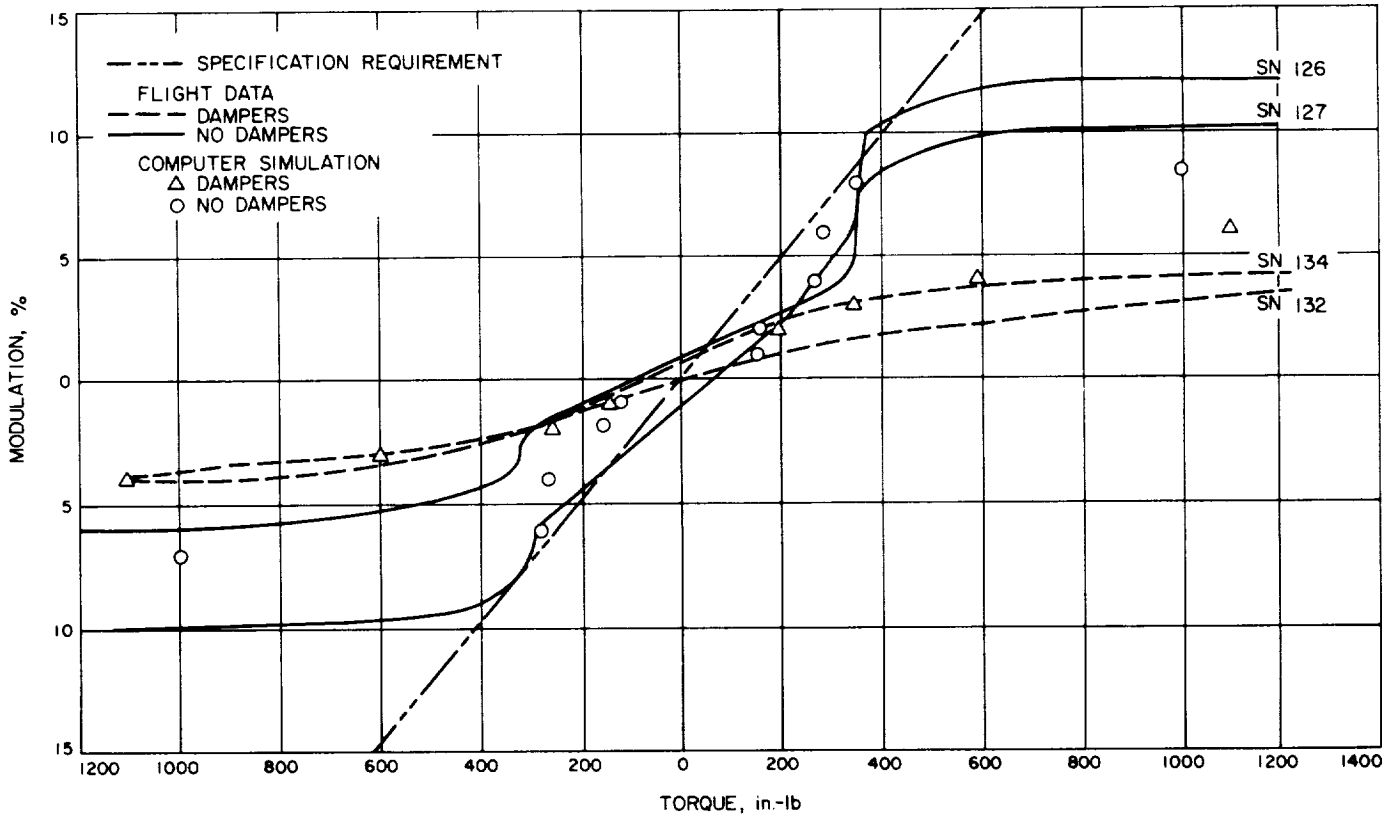

Fig. 6. Typical data, flight actuator hinge moment

Nomenclature (contd)

M_w	torque at worm shaft
N_1	input drive gear reduction
N_2	output drive gear reduction
R	drive motor armature resistance
$U(t)$	transport function
V_e	voltage input
α	worm lead angle
$\dot{\theta}_c$	clutch output shaft speed
$\dot{\theta}_e$	clutch input shaft speed
$\dot{\theta}_o$	output shaft speed
$\dot{\theta}_w$	worm shaft speed
μ_w	worm mesh friction